

# Second-order Dirac superconductors and magnetic field induced Majorana hinge modes

Sayed Ali Akbar Ghorashi<sup>1</sup>, Xiang Hu<sup>1</sup>, Taylor L. Hughes<sup>2</sup>, Enrico Rossi<sup>1</sup>

<sup>1</sup>Department of Physics, William & Mary, Williamsburg, Virginia 23187, USA and

<sup>2</sup>Department of Physics and Institute for Condensed Matter Theory, University of Illinois at Urbana-Champaign, IL 61801, USA

We identify three dimensional higher-order superconductors characterized by the coexistence of one-dimensional Majorana hinge states and gapless surface states. We show how such superconductors can be obtained starting from the model of a spinful quadrupolar semimetal with two orbitals and adding an s-wave superconducting pairing term. By considering all the possible s-wave pairings satisfying Fermi-Dirac statistics we obtain six different superconducting models. We find that for two of these models a flat-band of hinge Majorana states coexist with surface states, and that these models have a non-vanishing quadrupole-like topological invariant. Two of the other models, in the presence of a Zeeman term, exhibit helical and dispersive hinge states localized only at two of the four hinges. We find that these states are protected by combinations of rotation and mirror symmetries, and that the pair of corners exhibiting hinge states switches upon changing the sign of the Zeeman term. Furthermore, we show that these states can be localized to a single hinge with suitable perturbations. The remaining two models retain gapless bulk and surface states that spectroscopically obscure any possible hinge states.

The modern theory of polarization for crystalline insulators [1] has revealed that in crystals a dipole moment can be expressed in terms of Berry phases, and that a finite dipole necessarily implies the presence of boundary charges. The presence of nontrivial Berry phases and boundary states are the hallmarks of topological systems [2], and indeed it is now clear that there is a strong connection between the theory of topological insulators (TIs) and systems with quantized dipole moments [3–5]. This connection has led to the realization that the extension of the modern theory of polarization to higher multipole moments allows the identification of new classes of topological crystalline insulators [6, 7], termed “higher-order” TIs (HOTIs). Within this framework, a higher-order multipole TI of order  $m$  has a quantized nonzero electric  $m^{\text{th}}$ -pole in the bulk (with  $m = 1$  for a dipole,  $m = 2$  for a quadrupole,...) and localized charges at its  $d - m$ -dimensional boundaries,  $d$  being the insulator’s spatial dimension. Since the work of Refs. 6 and 7 many proposals of HOTIs of various types have been presented [8–12]. Higher-order topological insulating phases have been realized in metamaterial arrays [13–15], phononic systems [16], and it has been proposed that bismuth [10], strained SnTe [8], and some 2D transition metal dichalcogenides [17] are second-order TIs. In addition, there has been exciting new work on higher order topological superconductors (HOTSCs) and topological semimetals (HOTSMs) [9, 17–30].

In this work we identify for the first time a new class of higher-order topological superconductors: *second-order Dirac superconductors*, Fig. 1. Such novel three-dimensional (3D) higher-order topological superconductors exhibit the unique property to have both topologically protected Dirac cones for states at the surface ( $d-1$  boundary) and topologically protected dispersionless Majorana states at the hinges ( $d-2$  boundary). The hinge states can be interpreted as Majorana arcs joining the surface Dirac points. We explicitly show that this unique configuration of surface and hinge states is associated with a topological invariant that can be interpreted as the

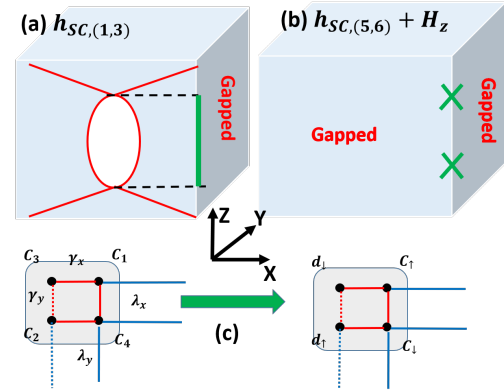


FIG. 1. Summary illustration of the models with hinge modes studied in this work. (a) model  $h_{SC,1}$  (rotate by  $C_4$  for model  $h_{SC,3}$ ). (b) models  $h_{SC,5}$ ,  $h_{SC,6}$  with magnetic field (Zeeman term  $H_z$ ) in the  $z$ -direction. Red lines represent surface states for  $k_{x,y} = 0$  cuts. Green lines represent flat-band hinge states; green crosses represent dispersive hinge nodes. (c) The unit cell convention used to convert between spinless and spinfull version of HOTI and HOTSM.

generalization to the superconducting case of the quadrupole moment. This model can provide a platform to study the interplay of the bulk, surface and hinge states on an equal footing which can significantly help towards understanding the transport properties of systems with higher-order topology. In addition, we identify 3D superconducting systems that can be driven into a higher-order topological state, exhibiting dispersive helical Majorana states at the hinges, simply via the application of an external magnetic field. Interestingly, we find that the hinges are localized at only two of the four hinges (see [23] and [31] for insulating examples of states localized at two corners). Furthermore, the pairs of corners where the Majorana modes are located can be selected by changing the sign of the magnetic field. We also show that by breaking diagonal/antidiagonal mirror symmetries, it is possible to drive the system into a unique topological state in which Majorana

states are present only at one of the hinges.

We start by considering a model for a topological quadrupolar semimetal constructed from layers of 2D quadrupolar topological insulators (TIs) [32]. Schematically, the unit cell for the tight binding model for the 2D quadrupolar insulator layer is illustrated in Fig. 1 (c). For each cell we have two orbitals ( $c$ ,  $d$ ) and a spin-1/2 degree of freedom, represented by the four black dots in Fig. 1 (c). Let  $\gamma_i$  ( $i = x, y$ ) be the intra-cell hopping amplitudes, red lines in Fig. 1 (c), and  $\lambda_i$  the inter-cell hopping, blue lines in Fig. 1 (c). Hopping processes represented by dotted lines have a phase that is opposite to the one of the hopping processes represented by solid lines. Depending on the choice of interlayer tunneling terms between 2D layers of quadrupolar TIs we obtain different Hamiltonians,  $H$ , for the resulting 3D system. In momentum space we have  $H_{SM} = \sum_{\mathbf{k}} \psi_{\mathbf{k}}^\dagger h_{SM}(\mathbf{k}) \psi_{\mathbf{k}}$ , where  $\psi_{\mathbf{k}}^T$  is the spinor  $(c_{\mathbf{k}\uparrow}, d_{\mathbf{k}\uparrow}, d_{\mathbf{k}\downarrow}, c_{\mathbf{k}\downarrow})$ , formed by the annihilation operators  $c_{\mathbf{k}\alpha}$ ,  $d_{\mathbf{k}\alpha}$ , for an electron in orbital  $c$ ,  $d$ , with spin  $\alpha$  and momentum  $\mathbf{k}$ , and  $h_{SM}$  is a  $4 \times 4$  Bloch Hamiltonian matrix of the general form:

$$h_{SM}(\mathbf{k}) = (\gamma_x + \chi_x(k_x) + \lambda_x \cos(k_x))\Gamma_4 + \lambda_x \sin(k_x)\Gamma_3 \\ + (\gamma_y + \chi_y(k_y) + \lambda_y \cos(k_y))\Gamma_2 + \lambda_y \sin(k_y)\Gamma_1. \quad (1)$$

In Eq. (1) all the lattice constants are taken to be 1,  $\chi_i(k_z)$  ( $i = x, y$ ) are periodic functions of  $k_z$  with forms fixed by the interlayer tunneling terms,  $\{\Gamma_\alpha\}$  are the  $4 \times 4$  matrices given by the direct product of  $2 \times 2$  Pauli matrices  $\sigma_i$ ,  $\kappa_i$  in spin and orbital space, respectively:  $\Gamma_0 = \sigma_3 \kappa_0$ ,  $\Gamma_i = -\sigma_2 \kappa_i$ ,  $\Gamma_4 = \sigma_1 \kappa_0$ . In the remainder we assume  $\chi_i(k_z)$ ,  $\gamma_i$ ,  $\lambda_i$  to be independent of the in-plane direction ( $x$  or  $y$ ) such that the normal state topological quadrupolar semimetal has  $C_4$  symmetry. To be explicit we will set  $\lambda_i = \lambda$  and use it as our unit of energy with  $\lambda = 1$ . We then set  $\chi_i(k_z) = \cos(k_z)/2$ , and  $\gamma_i = \gamma = -3/4$ . With this choice of parametrization,  $h_{SM}(\mathbf{k})$  has fixed  $k_z$  “momentum slices” with a non-vanishing quantized quadrupole moment for  $\cos(k_z) < -1/2$ , and vanishing quadrupole for  $\cos(k_z) > -1/2$ . As a consequence, the bulk bands are semimetallic with four-fold degenerate nodes at the locations  $k_z^{(c)}$  where the quadrupole changes, i.e.,  $\cos(k_z^{(c)}) = -1/2$  [32]. It is important to point out that any HOTSM with a well-defined nontrivial quadrupole moment and  $C_4$  and mirror symmetries should lead, in the presence of s-wave superconducting pairing, to results qualitatively similar to the one that we present below. The presence of the  $C_4$  and mirror symmetries is important, as we will show, to be able to “tune” the hinge states via external magnetic fields.

The most general mean-field Hamiltonian describing a superconducting state for our system is given by  $H_{SC} = \sum_{\mathbf{k}} \Psi_{\mathbf{k}}^\dagger h_{SC}(\mathbf{k}) \Psi_{\mathbf{k}}$  where  $\Psi_{\mathbf{k}}^T = (\psi_{\mathbf{k}}, \psi_{-\mathbf{k}}^\dagger)$  is the spinor in Nambu space and  $h_{SC}(\mathbf{k}) = \tau_3(h_{SM}(\mathbf{k}) - \mu) + \Delta_0^{(ij)}(\mathbf{k})\tau_2\sigma_i\kappa_j$ , where  $\mu$  is the chemical potential,  $\Delta_0^{(ij)}(\mathbf{k})$  the superconducting pairing strength in the  $(ij)$  spin orbital channel, and  $\{\tau_i\}$  are the Pauli matrices in Nambu space.

Model	$\Lambda_i$	$\mathcal{M}_x$	$\mathcal{M}_y$	$\mathcal{C}_4$	Structure	HOTSC
$h_{SC,1}$	$\sigma_1\kappa_2$	$\tau_3m_x$	$\tau_3m_y$	-	intra-S	✓
$h_{SC,2}$	$\sigma_2\kappa_1$	$\tau_0m_x$	$\tau_3m_y$	-	intra-S	✓
$h_{SC,3}$	$\sigma_2\kappa_0$	$\tau_3m_x$	$\tau_3m_y$	-	inter-S	✓
$h_{SC,4}$	$\sigma_2\kappa_3$	$\tau_3m_x$	$\tau_0m_y$	-	inter-T	✓
$h_{SC,5}$	$\sigma_0\kappa_2$	$\tau_3m_x$	$\tau_3m_y$	$\tau_0\hat{r}_4$	inter-S	-(✓*)
$h_{SC,6}$	$\sigma_3\kappa_2$	$\tau_0m_x$	$\tau_0m_y$	$\tau_3\hat{r}_4$	intra-T	-(✓*)

TABLE I. The pairings for the six different models discussed in this work. Columns 2-4 show the representation of the pairing term and of the symmetry operators for each model.  $m_x = \sigma_1\kappa_3$ ,  $m_y = \sigma_1\kappa_1$ ,  $\hat{r}_4 = \frac{i}{2}(\sigma_1 + i\sigma_2)\kappa_2 + \frac{1}{2}(\sigma_1 - i\sigma_2)\kappa_0$ . Column 6 shows the pairing structure: inter/intra and S/T are short for inter/intra orbital and spin singlet/triplet, respectively. Column 7 shows whether the model is a HOTSC: models with “\*” in the parenthesis denotes existence of HOTSC in the presence of magnetic field.

Restricting the superconducting pairing to be s-wave, i.e.,  $\Delta_0^{(ij)}(\mathbf{k}) = \text{const} = \Delta_0$ , we obtain

$$h_{SC,i} = \tau_3(h_{SM}(\mathbf{k}) - \mu) - \Delta_0\tau_2\Lambda_i \quad (2)$$

where  $\Lambda_i$  is a  $4 \times 4$  matrix, independent of  $\mathbf{k}$ , that determines the structure of the superconducting pairing in orbital and spin space. The requirement that the pairing term satisfies Fermi-Dirac statistics implies that there are only six possible pairing matrices  $\Lambda_i$ , listed in the second column of Table I, (see e.g., [33]). As a consequence, starting from  $h_{SM}$ , we can obtain six distinct s-wave superconducting states.

The normal state already has broken time-reversal symmetry ( $T^2 = -1$ ), when the superconducting pairing is added these superconductors belong to symmetry class  $D$  [2]. We note that, our model has a pseudo-chiral symmetry but its presence is not required for our results. All the models have mirror symmetries  $\mathcal{M}_x$ ,  $\mathcal{M}_y$ , and  $\mathcal{M}_z$ , and therefore overall inversion symmetry  $\mathcal{I} = \mathcal{M}_x\mathcal{M}_y\mathcal{M}_z$ . The representation matrices for the  $\mathcal{M}_x$  and  $\mathcal{M}_y$  mirror symmetries are shown in Table I, and the matrix for  $\mathcal{M}_z$  is the identity matrix. Models  $h_{SC,5}$ ,  $h_{SC,6}$ , retain  $C_4$  symmetry in the superconducting state with representation matrices given in Table I.

Let us consider the quasi-particle spectra in the weak pairing limit  $\Delta_0 < \mu$ . Explicitly, we choose  $\mu = 1$ ,  $\Delta_0 = 0.5$  and find that models  $h_{SC,1}$ ,  $h_{SC,3}$ ,  $h_{SC,6}$  are fully gapped in the bulk by the pairing term while  $h_{SC,2}$ ,  $h_{SC,4}$ ,  $h_{SC,5}$  are gapless (see SM [34]). Model  $h_{SC,2}$  ( $h_{SC,4}$ ) has gapless, bulk, quasi-particle states forming a nodal line/loop in  $k_x - k_z$  ( $k_y - k_z$ ) plane, and model  $h_5$  has 4 nodes in the  $k_x - k_y$  plane at  $k_z$  values away from any high-symmetry points. We see that models  $h_{SC,1}$  and  $h_{SC,3}$  have the same symmetry, the same representation for  $\mathcal{M}_x$  and  $\mathcal{M}_y$ , and have the same bulk spectra. Thus, they will have the same essential properties for our study, and henceforth we only consider  $h_{SC,1}$ . Additionally, models  $h_{SC,2}$  and  $h_{SC,4}$  are related by a unitary transformation and a  $C_4$  rotation around the  $z$ -axis so we will only consider  $h_{SC,2}$  from now on. While we have focused on particular values of  $\mu$  and  $\Delta_0$ , the results do not change qualitatively as

long as  $\Delta_0 < \mu$ , as is appropriate for the weak-pairing limit.

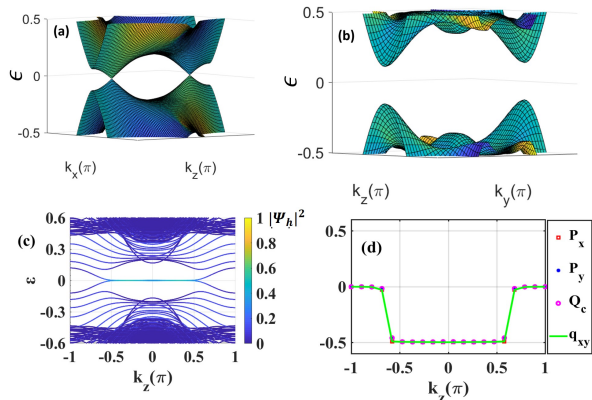


FIG. 2. The surface states of  $h_{SC,1}$  in (a)  $k_x - k_z$  and (b)  $k_y - k_z$  planes. (c) shows the Majorana hinges arc states in  $k_z$  direction. (d)  $P_x$ ,  $P_y$ ,  $Q_c$  and  $q_{xy}$  versus  $k_z$ .

We start by considering model  $h_{SC,1}$ . The pairing breaks  $C_4$  symmetry, while retaining mirror symmetries, so the bulk are completely gapped[6] (see supplementary material (SM) [34] for more detail). However, we find that the surfaces  $S_{y,\pm}$ , perpendicular to the  $y$ -axis, exhibit two gapless nodes per surface, Fig. 2 (a), whereas the ones perpendicular to the  $x$ -axis,  $S_{x,\pm}$ , are completely gapped, Fig. 2 (b). We then obtain the bands for the hinges and find, as shown in Fig. 2 (c), that dispersionless hinge Majorana states are present at the four corners of the  $xy$ -plane for values of  $k_z$  between the two gapless nodes on the  $S_y$  surface. In Fig. 2 (c) and all the other plots showing the spectrum of hinge states the color used for each point of the spectrum denotes the magnitude of the square of the corresponding eigenstate at the hinges  $|\Psi_h|^2$ . These states are reminiscent of the flat bands that appear between the nodes, and at the edges, of a 2D Dirac semimetal.

The structure of the spectrum and symmetry is similar to the one of the quadrupolar semimetal obtained in Ref. 32 when  $\gamma_i(k_z) \equiv \gamma_i + \chi(k_z)$  ( $i = (x, y)$ ) follow what in Ref. 32 is referred as path 2, and suggests that the presence of the boundary states, the hinge states in particular, might be due to a second-order topological invariant. To confirm it, we calculated (for details see SM [34]) the superconducting analog of the quadrupole moment  $q_{xy}(k_z)$  for each  $k_z$  slice. We have  $q_{xy}(k_z) \equiv (P_x(k_z) + P_y(k_z) - Q_c(k_z)) \bmod 1$  [6] where  $P_x(k_z)$ ,  $P_y(k_z)$  are the surface polarizations in the  $x$  and  $y$  directions, respectively, and  $Q_c(k_z)$  is the corner charge which takes values  $1/2, (0) \bmod 1$ , if hinge states are present (absent).

Fig. 2 (d) shows that  $P_x(k_z)$ ,  $P_y(k_z)$  are quantized, and that they take the non-trivial value  $-1/2$  for  $k_z$  in the interval between the two gapless nodes of the surfaces states on  $S_y$ , the same range of  $k_z$  for which we have hinge states. As a consequence we find that for values of  $k_z$  between the two surface nodes,  $q_{xy}(k_z)$  is also non-trivial and therefore that the hinge states in model  $h_{SC,1}$  are topologically protected and can be

captured by a second-order, quadrupole-like, topological invariant. Interestingly, we find that the presence of the gapless nodes on the surface, and of the hinge states, is not affected by perturbations that break both mirror symmetries, and thus the hinge states are perturbatively stable when the BdG particle-hole symmetry is maintained even when the mirror symmetry is broken (see SM [34]).

Due to the presence of Dirac nodes in the band structure of the surface states, and finite value of the quadrupole-like invariant we term superconductors like the one described by model  $h_{SC,1}$  (and  $h_{SC,3}$ ) *second order Dirac superconductors*. This is one of the main results of this work.

For models  $h_{SC,2,4}$  the gapless nature of the bulk and surface states leads to obscured hinge modes (see Fig. 2 in SM [34]).

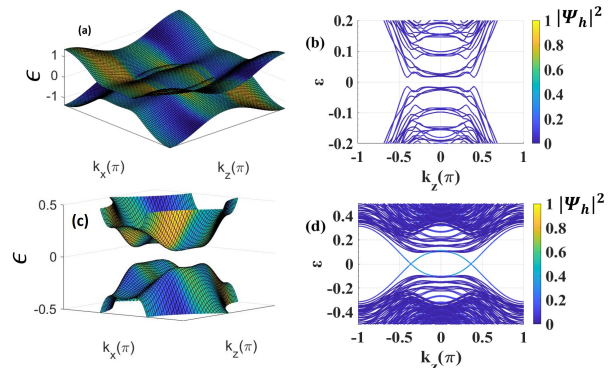


FIG. 3. Model  $h_{SC,5}$ : Surface states (a) in  $k_x - k_z$  plane, and hinge states (b) along  $k_z$ , when  $J_z = 0$ , (c) and (d), same as (a) and (b), respectively, for the case when  $J_z = 0.4$ .

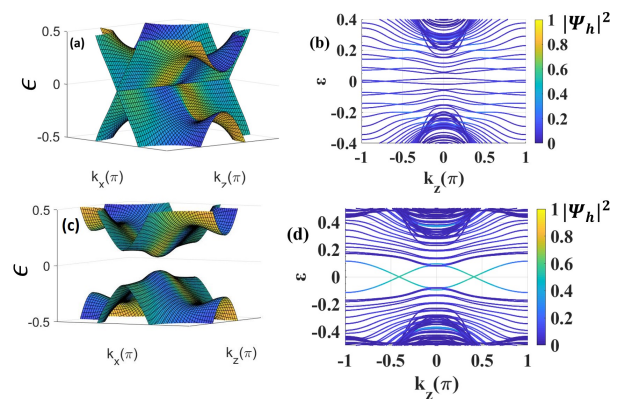


FIG. 4. Model  $h_{SC,6}$ : Surface states (a) in  $k_x - k_z$  plane, and hinge states (b) along  $k_z$ , when  $J_z = 0$ , (c) and (d), same as (a) and (b), respectively, for the case when  $J_z = 0.4$ .

Models  $h_{SC,5}$  and  $h_{SC,6}$  differ from the previous models in that, in addition to the mirror symmetries  $\mathcal{M}_x$  and  $\mathcal{M}_y$ , they retain the  $C_4$  symmetry of the original semimetal.

As mentioned, model  $h_{SC,5}$  has nodal points in the bulk quasi-particle spectrum, while  $h_{SC,6}$  is fully gapped in the

bulk (see SM [34]). We find that both models have gapless surface states but of different nature. Due to the  $C_4$  symmetry, we only show the results for the surface states  $S_{y,\pm}$ . The surface bands of model  $h_{SC,5}$  exhibit two nodal loops, see Fig. 3 (a), whereas the surface bands of model  $h_{SC,6}$  exhibit a nodal line at  $k_x = 0$  for the  $S_y$  surface states ( $k_y = 0$  for the  $S_x$  surface states), Fig. 4 (a). Figure 3 (b) and Fig. 4 (b) show the bands for the hinges for models  $h_{SC,5}$  and  $h_{SC,6}$  and we see that there are no interesting localized hinge modes present.

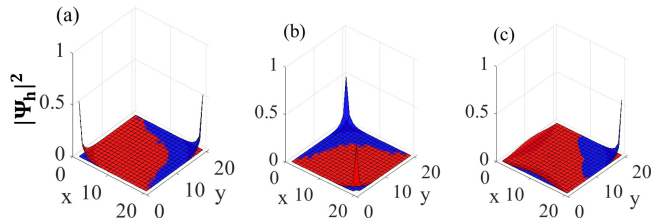


FIG. 5.  $|\Psi_h(x, y)|^2$  for model  $h_{SC,6}$  in the presence of a Zeeman term. We have two pairs of degenerate states. For each pair  $|\Psi_h(x, y)|^2$  is the same. In the figure we show in blue and red the two different  $|\Psi_h(x, y)|^2$  profiles. (a)  $J_z = 0.4$ ,  $k_z = 0.41\pi$ , value for which the helical hinge bands cross (Fig. 4 (d)). (b)  $J_z = -0.4$ ,  $k_z = 0.41\pi$ . (c)  $J_z = 0.4$  plus  $C_4\mathcal{M}_x$  breaking perturbation:  $0.1\tau_3r_4^{-1}m_x$ . In (c)  $k_z = 0.19\pi$ , for which we have the lowest positive energy.

However, an external magnetic field can perturb these systems to generate hinge modes. Let us apply a uniform magnetic field, or proximity-couple to a ferromagnet, to generate a Zeeman term  $H_z = J_z\tau_3\sigma_3\kappa_0$ , where  $J_z$  is directly proportional to the magnitude of the external magnetic field (we ignore any orbital effects of the magnetic field). This term qualitatively modifies the band structures of  $h_{SC,5}$  and  $h_{SC,6}$ . From Figs. 3 (c), 4 (c) we see that the presence of the Zeeman term gaps out the the surface states completely (it also gaps out the bulk nodes of  $h_{SC,5}$ ). Furthermore, we see the appearance of clear hinge states within the gap of the surface states, as shown in Fig. 3 (d) and Fig. 4 (d).  $H_z$  breaks  $C_4$  symmetry and both mirror symmetries, but leaves the products  $C_4\mathcal{M}_x$  (anti-diagonal mirror) and  $C_4\mathcal{M}_y$  (diagonal mirror) intact. Because of these symmetries, and contrary to the hinge states of the other models discussed in this work, the hinge states of  $h_{SC,5}$  and  $h_{SC,6}$  (with Zeeman) are: dispersive, non-chiral, and localized only at two of the four hinges related by  $C_2$  symmetry. In addition, we find that the pair of corners where the helical hinge states are localized switches upon a change of sign of the Zeeman term (e.g., switching the direction of the external magnetic field), see Fig. 5. This phenomenon could be useful for the experimental detection of these systems. We note that magnetic fields were also proposed to induce a HOTSC state in a completely different system with different properties in two dimensions [35].

For  $J_z > 0$  ( $J_z < 0$ ) there are two, counter-propagating modes at two of the four corners, and they are  $\pm$  eigenstates of  $C_4\mathcal{M}_y$  ( $C_4\mathcal{M}_x$ ). The hinge modes are perturbatively stable even in the absence of the two  $C_4\mathcal{M}_i$  symmetries as long as

particle-hole symmetry is preserved. However, the modes can be destroyed through bulk or surface phase transitions. Because the hinge states are located at opposite sides of the anti-diagonal (diagonal), the breaking of the  $C_4\mathcal{M}_x$  ( $C_4\mathcal{M}_y$ ) symmetry leads to non-symmetric hinge states and, for a strong enough  $C_4\mathcal{M}_x$  ( $C_4\mathcal{M}_y$ ) symmetry breaking perturbation, to the almost complete suppression of the hinge states at one corner and the enhancement of the hinge states at the opposite corner, as shown in Fig. 5 (c).

In conclusion, we have identified a new class of higher-order topological superconductors (HOTSCs): *second-order Dirac superconductors*. HOTSCs in this class have both topologically protected Dirac cones for states at the surface (d-1 boundary) and topologically protected dispersionless Majorana states at the hinges (d-2 boundary). The coexistence of gapless surface and hinge modes should lead to novel transport properties that it would be interesting to compare to the ones of conventional topological superconductors[2, 36–46]. We have then identified 3D superconducting systems that can be driven into a higher-order topological state simply via inclusion of a Zeeman term, having dispersive helical Majorana hinge states that are located at only two (or one) of the corners. We have shown that by varying the relative sign of the Zeeman term and of the mirror-diagonal symmetry-breaking perturbation, the position of the Majorana pairs can be tuned to be at a specific corner, leading to a highly tunable setup for realizing, and detecting, helical Majorana states.

S.A.A.G., X.H. and E.R. acknowledge support from ARO (Grant No. W911NF-18-1-0290), NSF (Grant No. DMR-1455233) and ONR (Grant No. ONR-N00014-16-1-3158). E.R. thanks the Aspen Center for Physics, which is supported by National Science Foundation grant PHY-1607611, for its hospitality during the early stages of the work. The numerical calculations have been performed on computing facilities at William & Mary which were provided by contributions from the NSF, the Commonwealth of Virginia Equipment Trust Fund, and ONR. TLH thanks the US National Science Foundation under grant DMR 1351895- CAR, and the MRSEC program under NSF Award Number DMR-1720633 (SuperSEED) for support.

- 
- [1] Raffaele Resta, “Macroscopic polarization in crystalline dielectrics: the geometric phase approach,” *Reviews of Modern Physics* **66**, 899–915 (1994).
  - [2] Ching-Kai Chiu, Jeffrey C. Y. Teo, Andreas P Schnyder, and Shinsei Ryu, “Classification of topological quantum matter with symmetries,” *Reviews of Modern Physics* **88**, 035005 (2016).
  - [3] J Zak, “Berry’s phase for energy bands in solids,” *Phys. Rev. Lett.* **62**, 2747 (1989).
  - [4] Taylor L Hughes, Emil Prodan, and B Andrei Bernevig, “Inversion-symmetric topological insulators,” *Phys. Rev. B* **83**, 245132 (2011).
  - [5] Ari M Turner, Yi Zhang, Roger SK Mong, and Ashvin Vishwanath, “Quantized response and topology of magnetic insula-

- tors with inversion symmetry,” *Phys. Rev. B* **85**, 165120 (2012).
- [6] Wladimir A Benalcazar, B Andrei Bernevig, and Taylor L Hughes, “Quantized electric multipole insulators,” *Science* **357**, 61–66 (2017).
- [7] Wladimir A Benalcazar, B Andrei Bernevig, and Taylor L Hughes, “Selected for a Viewpoint in Physics Electric multipole moments, topological multipole moment pumping, and chiral hinge states in crystalline insulators,” *Physical Review B* **96**, 245115 (2017).
- [8] Frank Schindler, Ashley M. Cook, Maia G. Vergniory, Zhijun Wang, Stuart S. P. Parkin, B. Andrei Bernevig, and Titus Neupert, “Higher-order topological insulators,” *Science Advances* **4**, eaat0346 (2018).
- [9] Zhida Song, Zhong Fang, and Chen Fang, “ $(d-2)$ -dimensional edge states of rotation symmetry protected topological states,” *Phys. Rev. Lett.* **119**, 246402 (2017).
- [10] Frank Schindler, Zhijun Wang, Maia G. Vergniory, Ashley M. Cook, Anil Murani, Shamashis Sengupta, Alik Yu. Kasumov, Richard Deblock, Sangjun Jeon, Ilya Drozdov, H el ene Bouchiat, Sophie Gu eron, Ali Yazdani, B. Andrei Bernevig, and Titus Neupert, “Higher-order topology in bismuth,” *Nature Physics* **14**, 918–924 (2018).
- [11] Motohiko Ezawa, “Higher-order topological insulators and semimetals on the breathing kagome and pyrochlore lattices,” *Phys. Rev. Lett.* **120**, 026801 (2018).
- [12] Motohiko Ezawa, “Minimal models for wannier-type higher-order topological insulators and phosphorene,” *Phys. Rev. B* **98**, 045125 (2018).
- [13] Jiho Noh, Wladimir A. Benalcazar, Sheng Huang, Matthew J. Collins, Kevin P. Chen, Taylor L. Hughes, and Mikael C. Rechtsman, “Topological protection of photonic mid-gap defect modes,” *Nature Photonics* **12**, 408–415 (2018).
- [14] Christopher W. Peterson, Wladimir A. Benalcazar, Taylor L. Hughes, and Gaurav Bahl, “A quantized microwave quadrupole insulator with topologically protected corner states,” *Nature* **555**, 346–350 (2018).
- [15] Stefan Imhof, Christian Berger, Florian Bayer, Johannes Brehm, Laurens W. Molenkamp, Tobias Kiessling, Frank Schindler, Ching Hua Lee, Martin Greiter, Titus Neupert, and Ronny Thomale, “Topoelectrical-circuit realization of topological corner modes,” *Nature Physics* **14**, 925–929 (2018).
- [16] Marc Serra-Garcia, Valerio Peri, Roman S ussstrunk, Osama R. Bilal, Tom Larsen, Luis Guillermo Villanueva, and Sebastian D. Huber, “Observation of a phononic quadrupole topological insulator,” *Nature* **555**, 342–345 (2018).
- [17] Motohiko Ezawa, “Simple model for second-order topological insulators and loop-nodal semimetals in Transition Metal Dichalcogenides  $XTe_2$  ( $X=Mo,W$ ),” arXiv e-prints, arXiv:1807.10932 (2018), arXiv:1807.10932 [cond-mat.mes-hall].
- [18] Josias Langbehn, Yang Peng, Luka Trifunovic, Felix von Oppen, and Piet W. Brouwer, “Reflection-symmetric second-order topological insulators and superconductors,” *Phys. Rev. Lett.* **119**, 246401 (2017).
- [19] Yuxuan Wang, Mao Lin, and Taylor L. Hughes, “Weak-pairing higher order topological superconductors,” *Phys. Rev. B* **98**, 165144 (2018).
- [20] Eslam Khalaf, “Higher-order topological insulators and superconductors protected by inversion symmetry,” *Phys. Rev. B* **97**, 205136 (2018).
- [21] Dumitru C alug aru, Vladimir Juri ci c, and Bitan Roy, “Higher-order topological phases: A general principle of construction,” *Phys. Rev. B* **99**, 041301 (2019).
- [22] Zhijun Wang, Benjamin J. Wieder, Jian Li, Binghai Yan, and B. Andrei Bernevig, “Higher-Order Topology, Monopole Nodal Lines, and the Origin of Large Fermi Arcs in Transition Metal Dichalcogenides  $XTe_2$  ( $X=Mo,W$ ),” arXiv:1806.11116.
- [23] Benjamin J. Wieder and B. Andrei Bernevig, “The Axion Insulator as a Pump of Fragile Topology,” arXiv:1810.02373.
- [24] Benjamin J. Wieder, Zhijun Wang, Jennifer Cano, Xi Dai, Leslie M. Schoop, Barry Bradlyn, and B. Andrei Bernevig, “Strong and ”Fragile” Topological Dirac Semimetals with Higher-Order Fermi Arcs,” arXiv:1908.00016.
- [25] Rui-Xing Zhang, William S. Cole, and S. Das Sarma, “Helical hinge majorana modes in iron-based superconductors,” *Phys. Rev. Lett.* **122**, 187001 (2019).
- [26] Qiyue Wang, Cheng-Cheng Liu, Yuan-Ming Lu, and Fan Zhang, “High-temperature majorana corner states,” *Phys. Rev. Lett.* **121**, 186801 (2018).
- [27] Zhongbo Yan, Fei Song, and Zhong Wang, “Majorana corner modes in a high-temperature platform,” *Phys. Rev. Lett.* **121**, 096803 (2018).
- [28] Chen-Hsuan Hsu, Peter Stano, Jelena Klinovaja, and Daniel Loss, “Majorana kramers pairs in higher-order topological insulators,” *Phys. Rev. Lett.* **121**, 196801 (2018).
- [29] Yanick Volpez, Daniel Loss, and Jelena Klinovaja, “Second-order topological superconductivity in  $\pi$ -junction rashba layers,” *Phys. Rev. Lett.* **122**, 126402 (2019).
- [30] Ya-Jie Wu, Junpeng Hou, Yun-Mei Li, Xi-Wang Luo, and Chuanwei Zhang, “In-plane Zeeman field induced Majorana corner and hinge modes in an  $s$ -wave superconductor heterostructure,” (2019), arXiv:1905.08896.
- [31] Wladimir A. Benalcazar, Tianhe Li, and Taylor L. Hughes, “Quantization of fractional corner charge in  $C_n$ -symmetric higher-order topological crystalline insulators,” *Phys. Rev. B* **99**, 245151 (2019).
- [32] Mao Lin and Taylor L. Hughes, “Topological quadrupolar semimetals,” *Phys. Rev. B* **98**, 241103 (2018).
- [33] Tatsuki Hashimoto, Shingo Kobayashi, Yukio Tanaka, and Masatoshi Sato, “Superconductivity in doped dirac semimetals,” *Phys. Rev. B* **94**, 014510 (2016).
- [34] Supplementary material.
- [35] Xiaoyu Zhu, “Tunable majorana corner states in a two-dimensional second-order topological superconductor induced by magnetic fields,” *Phys. Rev. B* **97**, 205134 (2018).
- [36] Liang Fu and Charles L Kane, “Probing neutral majorana fermion edge modes with charge transport,” *Phys. Rev. Lett.* **102**, 216403 (2009).
- [37] Liang Fu and Charles L Kane, “Josephson current and noise at a superconductor/quantum-spin-hall-insulator/superconductor junction,” *Phys. Rev. B* **79**, 161408 (2009).
- [38] Matthew S. Foster and Emil A. Yuzbashyan, “Interaction-mediated surface-state instability in disordered three-dimensional topological superconductors with spin  $su(2)$  symmetry,” *Phys. Rev. Lett.* **109**, 246801 (2012).
- [39] Matthew S. Foster, Hong-Yi Xie, and Yang-Zhi Chou, “Topological protection, disorder, and interactions: Survival at the surface of three-dimensional topological superconductors,” *Phys. Rev. B* **89**, 155140 (2014).
- [40] Sayed Ali Akbar Ghorashi, Seth Davis, and Matthew S Foster, “Disorder-enhanced topological protection and universal quantum criticality in a spin-3/2 topological superconductor,” *Phys. Rev. B* **95**, 144503 (2017).
- [41] Sayed Ali Akbar Ghorashi, Yunxiang Liao, and Matthew S. Foster, “Critical percolation without fine-tuning on the surface of a topological superconductor,” *Phys. Rev. Lett.* **121**, 016802 (2018).
- [42] Bitan Roy, Sayed Ali Akbar Ghorashi, Matthew S. Foster,

- and Andriy H. Nevidomskyy, “Topological superconductivity of spin-3/2 carriers in a three-dimensional doped luttinger semimetal,” *Phys. Rev. B* **99**, 054505 (2019).
- [43] Sayed Ali Akbar Ghorashi and Matthew S. Foster, “Criticality Across the Energy Spectrum from Random, Artificial Gravitational Lensing in Two-Dimensional Dirac Materials,” [arXiv:1903.11086](https://arxiv.org/abs/1903.11086).
- [44] Hong-Yi Xie, Yang-Zhi Chou, and Matthew S. Foster, “Surface transport coefficients for three-dimensional topological superconductors,” *Phys. Rev. B* **91**, 024203 (2015).
- [45] Shengyuan A. Yang, Hui Pan, and Fan Zhang, “Dirac and weyl superconductors in three dimensions,” *Phys. Rev. Lett.* **113**, 046401 (2014).
- [46] Haiping Hu, Fan Zhang, and Chuanwei Zhang, “Majorana doublets, flat bands, and dirac nodes in *s*-wave superfluids,” *Phys. Rev. Lett.* **121**, 185302 (2018).

## Second-order Dirac superconductors and magnetic field induced Majorana hinge modes SUPPLEMENTAL MATERIAL

### I. BULK SPECTRUM AND CONTINUUM ANALYSIS

We can analyze the bulk quasi-particle spectra by considering the effects of  $\Delta_0$  perturbatively on the normal state semimetal by using a continuum  $\mathbf{k} \cdot \mathbf{p}$  expansion around the nodes at the two  $k_z^{(c)}$ . The  $16 \times 16$  continuum Hamiltonian is

$$H_{\mathbf{k},\mathbf{p},i} = -\tau_3\pi_0\sigma_2(vk_x\kappa_3 + vk_y\kappa_1) + v_zk_z(\tau_3\pi_3\sigma_2\kappa_2 - \tau_3\pi_3\sigma_1\kappa_0) - \mu\tau_3\pi_0\sigma_0\kappa_0 - \Delta_0\tau_2\pi_1\Lambda_i \quad (3)$$

where  $\pi_i$  are Pauli matrices in the valley/node degree of freedom, and  $v, v_z$  are velocities ( $\hbar = 1$ ). In the nodal limit  $\mu \rightarrow 0$ , one can determine the nature of the bulk spectra by calculating how the pairing term commutes/anti-commutes with the kinetic terms.

In Fig 6, we present bulk band structures for all the models discussed in this work using the lattice model of Eq. (2) in the manuscript.

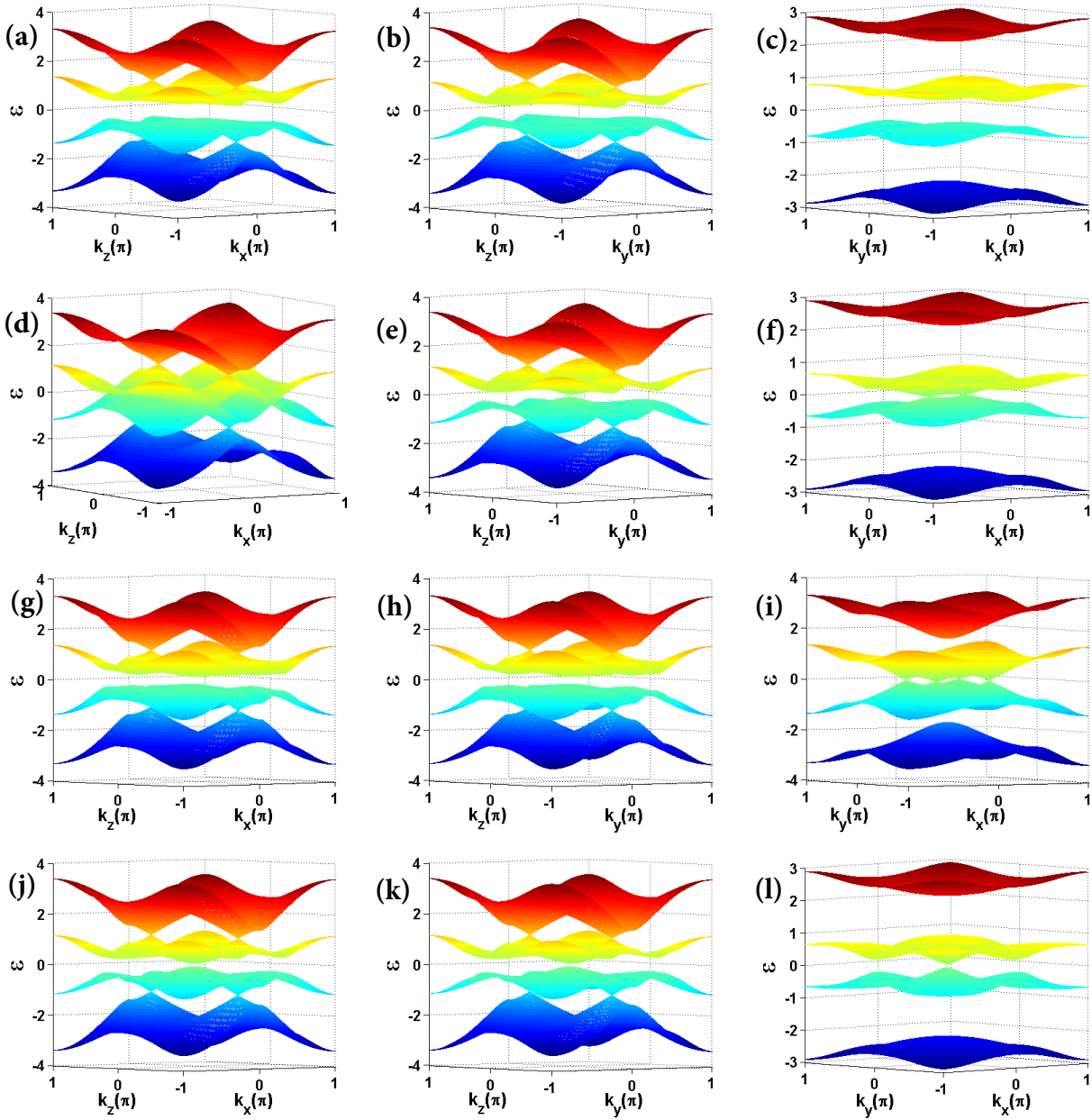


FIG. 6. Bulk spectrum for models  $h_{SC,1}$ ,  $h_{SC,2}$ ,  $h_{SC,5}$  and  $h_{SC,6}$  shown in the first, second, third and fourth rows, respectively. Each row, from left to right, represents  $k_x - k_z$  ( $k_y = 0$ ),  $k_y - k_z$  ( $k_x = 0$ ) and  $k_x - k_y$  ( $k_z = 0$ ) for all model except  $h_{SC,5}$  where  $k_z = 0.4$  is used plane.

#### MODEL $h_{sc,2}$

As mentioned in the manuscript the bulk states of model  $h_{SC,2}$  have nodal loops, (see Fig 6), and the surface states are gapless, as shown in Figs. 7 (a), (b). While we do find a small region of localized hinge states in the middle of the spectrum (see Fig. 7 (c)), the gapless bulk and surface states obscure them. It would be difficult to spectroscopically isolate the hinge modes of this model for any practical or experimental purpose. The same is true of model  $h_{SC,4}$ . Thus, as we noted in the manuscript, while there may be some interesting features of the gapless bulk and surface states of these models left to explore, we leave the study of these models for future works given that in this work our primary interest is in hinge-mode phenomenology.

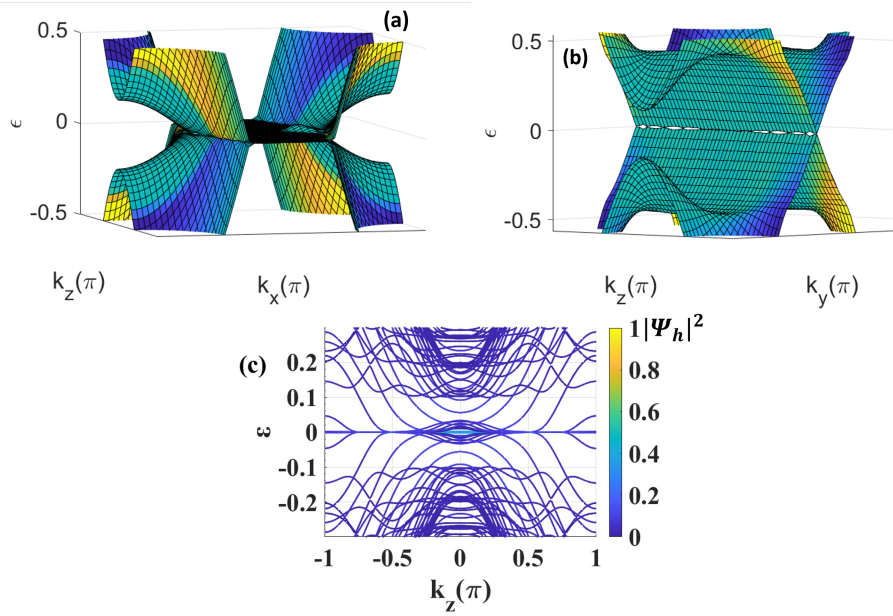


FIG. 7. The surface states of  $h_{SC,2}$  in (a)  $k_x - k_z$  and (b)  $k_y - k_z$  planes. (c) shows the Majorana hinges arc states in  $k_z$  direction.

### THE EFFECT OF SYMMETRY-BREAKING PERTURBATIONS

In this section we show that the hinges states corresponding to second-order topological superconductors of  $h_{SC,1}$  ( or  $h_{SC,3}$ ) are robust against mirror-symmetry breaking perturbations, and that the effect of the Zeeman term  $J_z$  on the obscured hinges states of models  $h_{SC,2}$  ( or  $h_{SC,4}$ ).

Figures 8(a) and (b) show the spectrum of hinge states for model  $h_{SC,1}$  in the presence of weak  $\mathcal{M}_x$  and  $\mathcal{M}_y$  breaking perturbations. As is evident hinge states are robust against weak symmetry-breaking perturbations and at most can partially remove degeneracies.

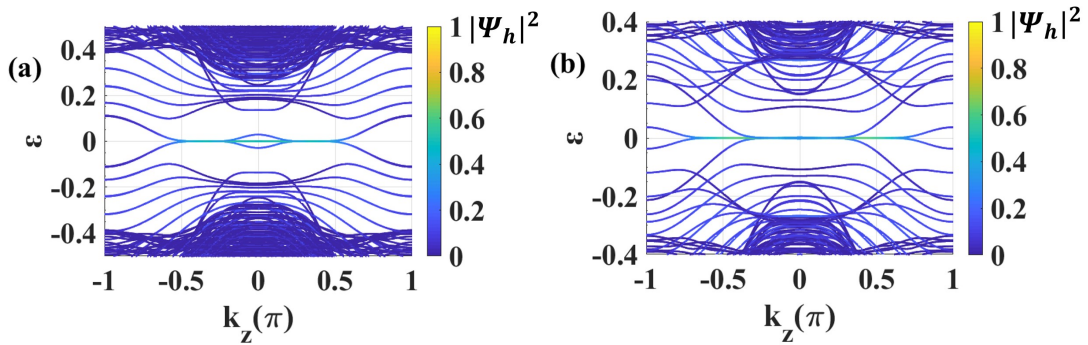


FIG. 8. The hinge states along  $k_z$ -direction for  $h_{SC,1}$  in the presence of (a)  $\mathcal{M}_x$  and (b)  $\mathcal{M}_y$  breaking perturbations.  $\mu = 1, \Delta_0 = 0.5$  and perturbation strength of 0.1 is used.

Fig. 9, shows the hinge spectrum for model  $h_{SC,2}$  in the presence of a magnetic field along the  $z$  direction,  $J_z$ , for two different values of  $J_z$ . We observe that the Zeeman term can only gradually remove some of the gapless points. We could not find any weak perturbation that can fully gap out the hinges states while preserving particle-hole symmetry.

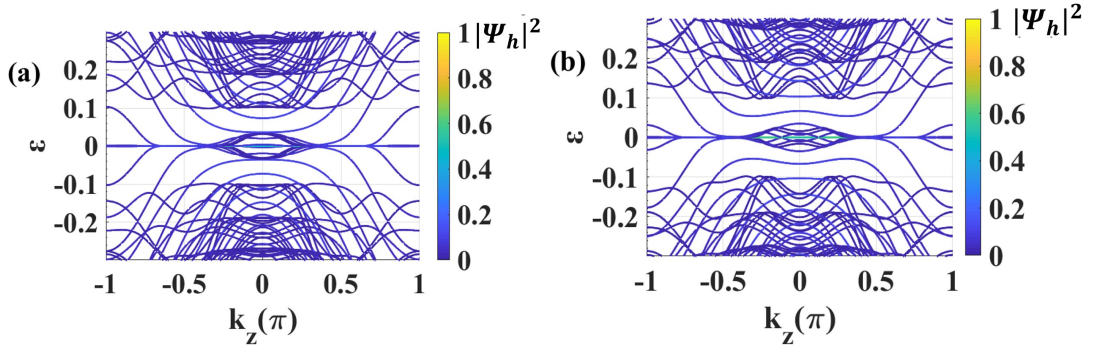


FIG. 9. The hinge states along  $k_z$ -direction for  $h_{\text{SC},2}$  in the presence of the Zeeman terms with (a)  $J_z = 0.4$  and (b)  $J_z = 0.6$ .  $\mu = 1$ ,  $\Delta_0 = 0.5$  is used.

### THE CALCULATION OF THE QUADRUPOLE-LIKE INVARIANT FOR THE SECOND-ORDER DIRAC SUPERCONDUCTORS

For each superconducting Hamiltonian with two orbitals and one spin degree of freedom  $H_{\text{SC},i} = \Psi_{\mathbf{k}}^\dagger (\tau_3 h_{\text{SM}}(\mathbf{k}) - \Delta_0 \tau_2 \Lambda_i) \Psi_{\mathbf{k}}$ , we can substitute the original basis  $\Psi_{\mathbf{k}} = (c_{\mathbf{k}\uparrow}, d_{\mathbf{k}\uparrow}, c_{\mathbf{k}\downarrow}, d_{\mathbf{k}\downarrow}, c_{-\mathbf{k}\uparrow}^\dagger, d_{-\mathbf{k}\uparrow}^\dagger, c_{-\mathbf{k}\downarrow}^\dagger, d_{-\mathbf{k}\downarrow}^\dagger)^T$  with a new basis  $\tilde{\Psi}_{\mathbf{k}} = (c_{\mathbf{k}\uparrow}, d_{\mathbf{k}\uparrow}, c_{\mathbf{k}\downarrow}, d_{\mathbf{k}\downarrow}, \tilde{c}_{\mathbf{k}\uparrow}, \tilde{d}_{\mathbf{k}\uparrow}, \tilde{c}_{\mathbf{k}\downarrow}, \tilde{d}_{\mathbf{k}\downarrow})^T$ , where  $\tilde{c}$  and  $\tilde{d}$  are two additional electron orbitals. Now we have a Hamiltonian with the pure electron basis

$$\tilde{H}_i = \sum_{\mathbf{k}} \tilde{\Psi}_{\mathbf{k}}^\dagger (\tau_3 h_{\text{SM}}(\mathbf{k}) - \Delta_0 \tau_2 \Lambda_i) \tilde{\Psi}_{\mathbf{k}}. \quad (4)$$

The formulation of the original BdG Hamiltonian in terms of purely electronic degrees of freedom makes direct the connection between the quadrupole moment of non-superconducting systems and the equivalent ‘‘quadrupole moment’’ that can be used to identify higher order topological superconducting states.

The calculation of the polarization and quadrupole for model  $h_{\text{SC},1(3)}$  is carried out using the method presented in Ref.[7]. As stated in the main text we have  $q_{xy}(k_z) \equiv (P_x(k_z) + P_y(k_z) - Q_c(k_z)) \bmod 1$ , where  $q_{xy}$  is the quadrupole moment,  $P_x(k_z)$ ,  $P_y(k_z)$  are the surface polarizations in the  $x$  and  $y$  directions, respectively, and  $Q_c(k_z)$  is the corner charge which takes values  $1/2, (0) \bmod 1$ , if hinge states are present (absent). To obtain the edge-localized polarization  $P_x(k_z)$  for a fixed  $k_z$ , we place the Hamiltonian  $\tilde{H}_{1(3)}(k_z)$  in a geometry which is open in the  $y$  direction and periodic in the  $x$  direction. We have  $P_x = \sum_{R_y=N_y-N_l+1}^{N_y} p_x(R_y)$ , where  $R_y$  is a site along  $y$  in the discretized model,  $N_y$  is the size of the system along the  $y$  direction (in number of sites of the discretized model),  $N_l$  is the finite thickness of the edge layer used in the calculation, and (see Eqs.(5.8) and (5.9) of Ref.[7]):

$$p_x(R_y) = \sum_j \rho^j(R_y) \nu_x^j; \quad (5)$$

where

$$\rho^{j,R_x}(R_y) = \frac{1}{N_x} \sum_{k_x, \alpha} |[u_{k_x}^n]^{R_y, \alpha} [\nu_{k_x}^j]^n|^2, \quad (6)$$

In the equations above  $j$  and  $\nu_x^j$  are the index and eigenvalue for the Wilson loop along  $k_x$ , respectively,  $R_x$  and  $R_y$  are the position in  $x$  and  $y$  directions.  $N_x$  is the size in  $x$  direction,  $[\nu_{k_x}^j]^n$  represent the  $n$ -th component of the  $j$ -th Wannier function, and  $[u_{k_x}^n]^{R_y, \alpha}$  is the component of the  $n$ -th Bloch wave function at  $R_y$  with orbital index  $\alpha$ .  $P_y$  is obtained in a similar way via the substitutions  $x \rightarrow y$ ,  $y \rightarrow x$ . We calculate the corner charge using open boundary conditions both in the  $x$  and  $y$  direction:

$$Q_c = \sum_{R_x=N_x-N_l+1}^{N_x} \sum_{R_y=N_y-N_l+1}^{N_y} \rho(\mathbf{R}), \quad (7)$$

where  $\rho(\mathbf{R})$  is the charge density due to the occupied states.

In our calculations, we used  $N_x = 50$ ,  $N_y = 50$ ,  $N_z = 19$  and  $N_l = 10$ . For the bulk Hamiltonian, four bands are occupied. The values of the other parameters are the ones stated in the main text. When calculating the quadrupole moment for model  $h_{SC,1}$  we add a small perturbation of the form

$$\delta\tilde{H}_1 = 0.005\tau_0\Gamma_0 + 0.010(\tau_3\sigma_1\kappa_1 + \tau_3\sigma_0\kappa_3). \quad (8)$$

in order to fix the sign of  $P_x$ ,  $P_y$  and  $Q_c$  (i.e. to remove the ambiguity due to the fact that these quantities are well defined only up to  $\text{mod } 1$ ).